

Integrating SAR and optical imagery for regional mapping of paddy rice attributes in the Poyang Lake Watershed, China

Nathan Torbick, William Salas, Xiangming Xiao, Pete Ingraham, Matthew G. Fearon, Chandrashekhar Biradar, Delong Zhao, Ying Liu, Peng Li and Yonglin Zhao

Abstract. The development of agricultural monitoring tools is a focus of the Group on Earth Observations for the Global Earth Observation System of Systems (GEOSS). This requires combining synthetic aperture radar (SAR) and optical satellite sensors to provide more meaningful information in an operational context. The goal of this research was to characterize paddy rice agro-ecological attributes in an operational context. A decision tree framework combined multitemporal and multiscale PALSAR, MODIS, and Landsat observations to map rice extent, hydroperiod, crop calendar, and cropping intensity. The study was carried out in the Poyang Lake Watershed, Jiangxi Province, China. A multiseason field campaign was carried out to calibrate algorithms and validate the rice maps. The field data corresponded relatively well with the remote sensing metrics and validation found that the derived rice paddy maps possessed a high overall accuracy of 89%. The rice maps indicate that the watershed has 25% rice agriculture with 85% of all paddies undergoing a double-crop management pattern. Remotely sensed metrics showed that inundation periods for early rice were typically twice as long as inundation periods between crops, which corresponded to site level measurements at double crop locations. Using hydroperiod and crop intensity information a crop calendar indicated that the day of year (DOY) planting and harvesting activities was typically around DOY 77 and 329, respectively. The automated approach combining SAR and optical platforms with continental-scale acquisition strategies might allow for large-area, operational agricultural rice mapping. This can contribute to a GEOSS framework for improved agricultural monitoring.

Résumé. Le développement d'outils pour le suivi de l'agriculture constitue l'un des objectifs du Groupe sur les observations de la Terre du Système mondial des systèmes d'observation de la Terre (GEOSS). À cette fin, une combinaison de capteurs satellitaires radar à synthèse d'ouverture (RSO) et optiques est nécessaire pour fournir plus d'information substantielle dans un contexte opérationnel. Le but de cette recherche était de caractériser les attributs agro-écologiques du riz dans un contexte opérationnel. On a combiné dans un contexte d'arbre de décision des données d'observations multitemporelles et multi-échelles de PALSAR, MODIS et de Landsat pour cartographier les superficies de riz, l'hydropériode, le calendrier des cultures ainsi que l'intensité des cultures. L'étude a été réalisée dans le bassin du lac Poyang, dans la province de Jiangxi, en Chine. Une campagne de terrain échelonnée sur plusieurs saisons a été réalisée pour étalonner les algorithmes et valider les cartes de culture du riz. Les données de terrain correspondent relativement bien avec les mesures de télédétection et la validation a permis de trouver que les cartes des rizières affichaient une précision globale élevée de 89%. Les cartes de culture du riz indiquent que 25% du bassin versant est consacré à la riziculture et que 85% de toutes les rizières sont exploitées dans un contexte de gestion à double culture. Les mesures de télédétection ont montré que les périodes d'inondation pour le riz précoce étaient généralement deux fois plus longues que les périodes d'inondation entre les cultures, correspondant ainsi aux mesures effectuées au sol sur les sites à double culture. À l'aide des informations sur les hydropériodes et l'intensité des cultures, un calendrier des récoltes montre que le jour de l'année où ont lieu les activités de semence et de récolte se situait généralement environ entre les jours 77 et 329 de l'année. L'approche automatisée combinant les plateformes RSO et optiques avec des stratégies d'acquisition à l'échelle continentale pourrait permettre la cartographie à grande échelle et opérationnelle de la culture du riz. L'approche pourrait constituer un apport au programme GEOSS pour l'amélioration du suivi de l'agriculture.

[Traduit par la Rédaction]

Received 30 March 2010. Accepted 3 June 2010. Published on the Web at <http://pubs.casi.ca/journal/cjrs> on 4 October 2011.

N. Torbick¹, W. Salas, P. Ingraham, and M.G. Fearon. Applied Geosolutions, 87 Packers Falls Rd, Durham, NH 03857, USA.

X. Xiao, C. Biradar, and D. Zhao. Department of Botany and Microbiology & Center for Spatial Analysis, University of Oklahoma, Norman, Ok 73019, USA.

Y. Liu, P. Li, and Y. Zhao. Department of Geography, Jiangxi Normal University, Nanchang, China.

¹Corresponding author (e-mail: torbick@agsemail.com).

Introduction

Using synthetic aperture radar (SAR) to improve agricultural monitoring is a current focus of the Group on Earth Observations, and its integration is an element of the Global Earth Observation System of Systems (GEOSS). For large-area agricultural monitoring, systems that integrate sensors, spatial scales, and temporal resolutions to provide meaningful information in automated approaches are desired (Justice and Becker-Reshef, 2007; Parihar, 2009). Rather than focus on the technical development of a single sensor or data extraction method, operational approaches that combine disparate data to generate more meaningful information are becoming central components of agriculture monitoring systems (i.e., Pradhan, 2001; Xiao et al., 2005; Erasmi and Twele, 2009; McNairn et al., 2009; Torbick et al., 2010).

Rice is an extremely important crop given that it is the predominant food staple in many regions of the Earth. Rice paddies occupy nearly 11% of arable land with approximately half a billion tons of milled rice produced annually. Rice crops influence food security and regional economies, climate and hydrological resources, and the livelihoods of millions of people (IPCC, 1992; Li et al., 2005; Salas et al., 2007; Torbick et al., 2010).

In the past decade many studies have highlighted the advantages of SAR for rice paddy mapping. Currently as part of Japan Aerospace Exploration Agency's (JAXA) Kyoto & Carbon Initiative (K&CI), the Advanced Land Observing Satellite (ALOS) Phased Array L-band Synthetic Aperture Radar (PALSAR) acquisition strategy has been developed with a goal of having spatially and temporally consistent data at continental scales with adequate revisit frequency and timing to enable the development of large-area, operational rice monitoring. Concordantly, the moderate resolution imaging spectroradiometer (MODIS) collects observations in the optical spectral domain for the entire Earth at a near-daily temporal frequency. These systematic collection strategies provide an opportunity to contribute to the GEOSS framework and advance current agriculture monitoring systems.

The scientific goal of this research was to generate rice information (rice extent, number of crops, crop calendar) and to develop an operational rice monitoring system using both PALSAR and optical measurements. The project was carried out at a regional scale in the Poyang Lake Watershed (PLW) in Jiangxi Province, China. The technical objective of this study was to combine PALSAR and optical data for operational rice monitoring. The geospatial products generated from the rice monitoring system include maps of paddy rice extent, crop intensity (the number of crops within a given period, i.e., calendar or cropping year), crop calendar, and hydroperiod (the flood frequency and duration of flooding for a paddy field).

Methods

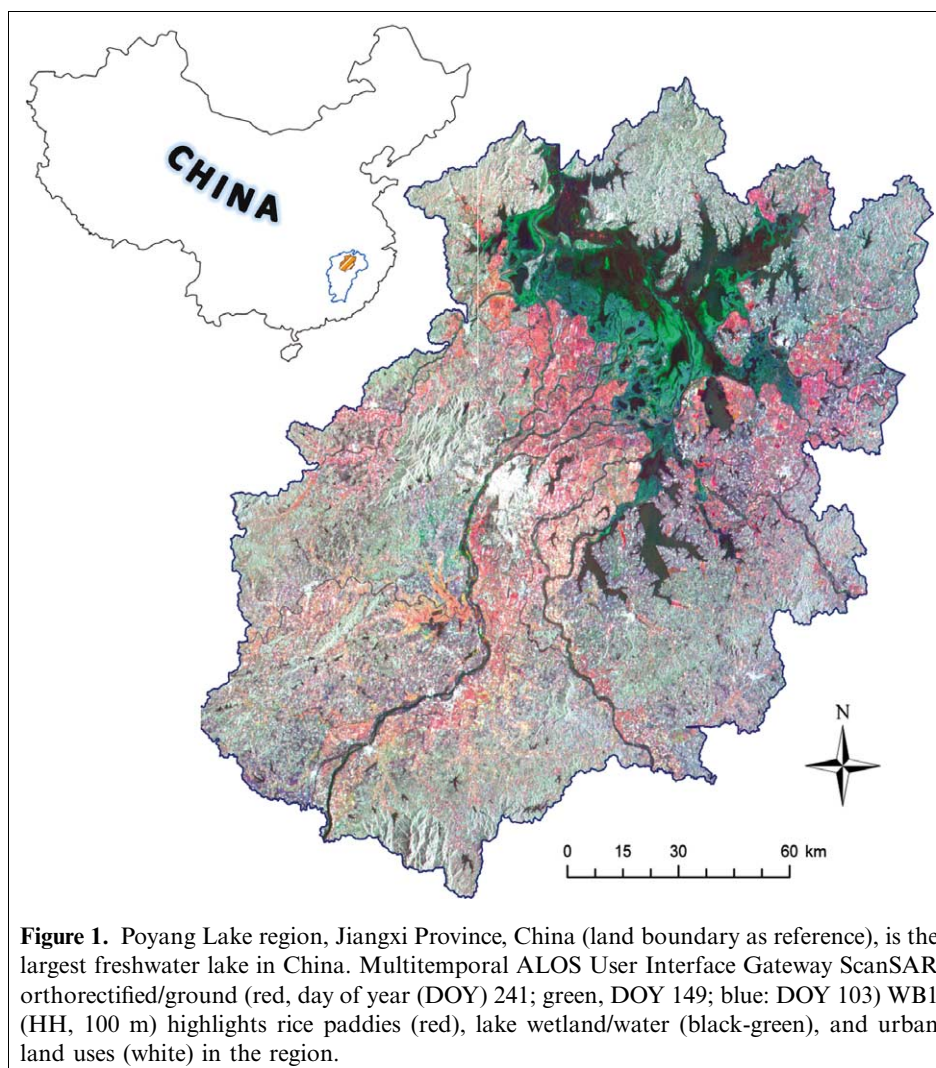
Study area

The PLW is located in the north central portion of Jiangxi Province, China (116.1W, 28.7N) (**Figure 1**). Government policies promoting economic growth and agriculture production have substantially altered the landscape in the watershed during the past half century (NBS, 2000). Land-use change analysis has shown reported land-use percentages to vary significantly and, by recent estimates, about half the region is considered farmland (Rao et al., 2002; Liu et al., 2005; Jiang et al., 2008). Rice paddies are dispersed around the lake primarily on the southern boundaries. The region has an average annual precipitation of 170 cm and an annual average temperature of 17 °C.

The PLW study area is approximately 23 500 km². Shuttle Radar Topography Mission (SRTM, Jarvis et al., 2008) data was used to create a digital elevation model (DEM) to delineate the study area. We generated a watershed boundary using void filler SRTM products to define the PLW based on flow, area, and accumulation patterns. The PLW study area has extremely dynamic hydrology with periodic flooding from central Yangtze River basin fluctuations and widespread levee systems altering flows. The levee system continues to develop and is used for flood control and paddy irrigation. Jiang et al. (2008) reported that in 1998 approximately 64 000 km of levees existed in the region. The dynamic hydrology and natural wetlands in the PLW pose a challenge for rice mapping as these land covers can have a similar phenology.

Field campaign

To calibrate and validate rice maps, a field campaign to collect agro-ecological attributes was carried out at five different double-crop (two rice plantings and harvests within one year) rice paddies. Sites were visited approximately once every 8 days between day of year (DOY) 133 and 312. All five paddy sites were categorized as irrigated rice paddies as opposed to rainfed sites, which are very rare in this watershed. The five unique rice paddy sites represent the conditions at the landscape scale as the region has similar management and cropping practices (i.e., transplanting, irrigation, and time of harvest). At each paddy, five 60 cm × 60 cm plot-level quadrats were sampled in a hierarchical approach. In each quadrat, sampling was repeated three times to generate an average of biomass and water depth. Within each quadrat 10–15 clusters (rice stalk groupings) were extracted. Within each cluster approximately 9–16 individual plants were weighed. Root, above-ground fresh haulm weight (g), and aboveground dry weight (g) biomass were obtained. A density-adjusted average biomass (i.e., fresh haulm weight) (g) was then generated to scale-up to the remote sensing imagery from the plot-level field measurements. Water depth measurements were



collected once every 8 days. Every 8 days, an average of three samples for each quadrat were generated at each site.

Georeferenced ground truth data were collected to validate the rice extent map. The south and central boundaries of the lake were identified as primary sites that were of interest and that were near the city of Nanchang. A stratified-random clustering approach was carried out following a well-established sampling protocol (Congalton and Green, 1999). To provide a statistically rigorous validation set, points were distributed along the local road network and the landscape where rice, wetlands, riparian areas, and other land covers were intermixed.

GPS field photos were collected in all directions for a given point to represent the patch rather than using a coordinate point. Keyhole markup language (KML) files were created to store and display points and photos on Google Earth. KML files use a tag-based structure with attributes that allow display. These photos are available for viewing in Google Earth at <http://www.comf.ou.edu/>; at this website users can search and share a library of global georeferenced field photos for product validation. Photos

and land covers were interpreted at a total of 320 points with a focus on rice and wetlands as these are typically the most confused classes. The field photos also focused on aquatic habitats as part of another study investigating duck migration and avian influenza (Gilbert et al., 2008). With unique samples at each of the sites a total of 320 validation points were utilized to construct a simple 2×2 error matrix for accuracy assessment.

Satellite data

A complementing suite of multitemporal and multiscale satellite observations, including ALOS PALSAR ScanSAR, MODIS, and Landsat 7 Enhanced Thematic Mapper Plus (ETM+), were used in combination. ALOS orbits in a Sun-synchronous pattern at an altitude of 691.65 km and at an inclination of 98.16° . The instrument features a wide-swath ScanSAR mode with single polarization. The center frequency is 1270 MHz (23.6 cm), with 14 MHz bandwidth in ScanSAR mode. In 5-beam ScanSAR mode, the incidence angle range varies from 18.0° to 43.0° . Ground

Table 1. SAR and optical imagery used to generate paddy rice attribute maps for the Poyang Lake watershed for 2007.

Sensor	Spatial	Spectral	Temporal	Scenes
Landsat	30 m	visual-shortwave infrared	Once	1
PALSAR	100 m	HH	42-day	10
MODIS	500 m	visual-shortwave infrared	8-day	46

resolutions depend on mode and include square 100 m spatial resolution pixels for ScanSAR stamps (small footprints) and 50 m × 70 m pixels for ScanSAR strips (longer footprints) in the azimuth and range direction, respectively. Absolute radiometric accuracy is < 1.5 dB between orbits (Rosenqvist et al., 2004).

In this study we used the stamp resolutions to develop the operational rice mapping from early PALSAR observations that were first available to the K&CI Science Team. The current PALSAR acquisition strategy includes ScanSAR Wide-Beam 1 (WB1; 100 m HH) acquisitions every 46 days for regional mapping of rice agricultures. Adjacent ScanSAR acquisitions overlap 50%, so effectively there have been two acquisitions every 46 days contiguously since October 2006. In this study we focus on the use of HH polarization because the ALOS acquisition strategy is collecting the ScanSAR strips for continental scale mapping and monitoring. We sought to develop an operational approach that could be applied for large-area monitoring.

High (temporal) frequency optical data were obtained from the MODIS instrument onboard the Terra (descending) and Aqua (ascending) satellite platforms. The MODIS sensor collects measurements in 36 spectral bands every 1–2 days at spatial resolutions of 250–1000 m. MODIS products are available from the Land Processes Distributed Active Archive Center. This study used the MOD09A1 L2G product (Vermote et al., 2002) that has been corrected for atmospheric attenuation. MOD09A1 data are 8-day surface reflectance of bands 1 (620–670 nm), 2 (841–876 nm), 3 (459–479 nm), 4 (545–565 nm), 5 (1230–1250 nm), 6 (1628–1652 nm), and 7 (2105–2155 nm) at 500 m resolution. The 8-day composite product uses the optimal observations considering frequency coverage, view angle, clouds, and aerosol loading.

A single Landsat 7 ETM+ scene was utilized. The ETM+ sensor collects spectral information in eight bands at 15, 30, and 60 m resolutions at 16-day repeat intervals. The Landsat image date (10 August 2007) was chosen in this project to match the high water (Poyang Lake) season while considering the PALSAR and MODIS time series. ETM+ data were obtained from Global Land Cover Facility Earth Science Data Interface. Data were resampled using cubic convolution algorithms, then orthorectified and delivered in the universal transverse mercator (UTM) projection as a GeoTiff. Poyang Lake is covered by World Reference System (WRS) path/row 121/40.

Image preprocessing and indices

This study utilized PALSAR imagery available from the Alos User Interface Gateway (AUIG 3.0) operated by JAXA. Imagery was obtained as unsigned 16-bit processed level 1.5 originally in CEOS format. Level 1.5 is defined by generic radiometric and geometric corrections performed according to specified map projections after performing range and multilook azimuth compressions (ERSDAC, 2006). At the JAXA Earth Observation Center, ScanSAR WB1 measurements were resampled using a bilinear scheme to project into the UTM Zone 10 North coordinate system. Additional radiometric adjustments were executed following the cosine of the zenith angle approach (Liang, 2005) to correct for viewing geometry affects; no further local incident angle corrections were needed as the study area and classification target (i.e., rice paddies) are extremely flat, and fields in this region are large and continuous. Scripts performed multiple tasks and transformed data into geotiffs of sigma nought σ^0 (Equation (1)). Ten ScanSAR scenes within the 2007 calendar rice season were used in this study.

$$\sigma^0 = 10 \log_{10}(\text{DN}^2) + \text{calibration factor} \quad (1)$$

MODIS preprocessing reprojected data into a common UTM projection and MODIS QAQC (MCD43A2) flags were used to identify potentially contaminated pixels. Contaminated pixels were removed from the analyses. A series of high temporal frequency indices were generated from the MODIS data. The land surface water index (LSWI) (Equation (2)) utilizes the sensitivity to moisture of shortwave infrared (SWIR) and has previously been used to assess ecological conditions and flood dynamics (Xiao et al., 2005). The enhanced vegetation index (EVI) (Equation (3)) builds on previous indices that measure vegetative surface conditions by incorporating information from the blue band's (MODIS blue band = 459–479 nm) sensitivity to atmosphere and coefficients adjusting for soil and background effects (Huete et al., 2002). An established relationship between LSWI and EVI was applied to map flooded regions.

$$\text{LSWI} = \frac{p_{\text{nir}} - p_{\text{swir}}}{p_{\text{nir}} + p_{\text{swir}}} \quad (2)$$

$$\text{EVI} = 2.5 \left(\frac{p_{\text{nir}} - p_{\text{swir}}}{p_{\text{nir}} + 6p_{\text{red}} - 7.5p_{\text{blue}} + 1} \right) \quad (3)$$

$$\text{MODIS flood} = \text{LSWI} + 0.05 > \text{EVI} \quad (4)$$

where p is reflectance.

A temporary inversion of the vegetation indices within a plant growing season, where LSWI values either approach or are higher than EVI values, signals flooding in paddy rice fields. To slightly relax the simple threshold assumption an adjustment factor is included (Xiao et al., 2005). In this study flood characterization was determined using the

relationship between LSWI and EVI (Equation (4)). This algorithm has been successfully implemented to map rice paddies in China (Xiao et al., 2005), South and Southeast Asia (Xiao et al., 2006), and California, USA (Torbeck et al., 2010).

The 30 m resolution Landsat imagery is more capable of capturing fine-scale meandering coastlines and tributaries compared with MODIS (250 m) or ScanSAR WB1 (100 m) imagery. The Landsat ETM+ scene (10 August 2007) was radiometrically converted from digital numbers (DN) to spectral radiance to top-of-atmosphere reflectance (Equations (5), (6)). A Landsat ETM+ lake mask was created using the Landsat LLSWI. Here, Landsat LLSWI uses spectral information in the near infrared (NIR, 0.75–0.90 μm) and SWIR (1.55–1.75 μm), which is sensitive to moisture or water content. Generally, the index increases as moisture or water increases. A region growing-majority filter was used to overcome scan line corrector (SLC) stripping by smoothing over gaps caused by SLC stripping. A binary map of open water and nonwater was created as a Landsat-scale water mask.

$$\text{Radiance} = \frac{\text{LMAX} - \text{LMIN}}{255 * \text{DN} + \text{LMIN}} \quad (5)$$

where LMAX and LMIN are the spectral radiances for each band obtained from the U.S. Geological Survey calibration files for 1G products, and

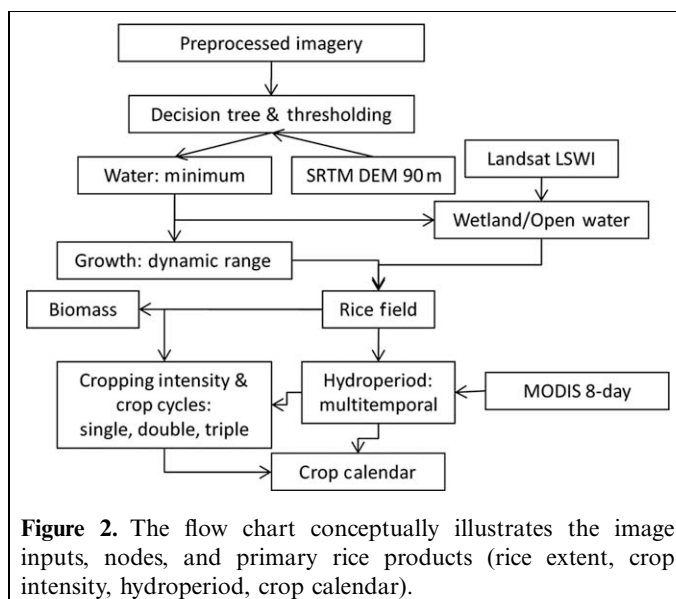
$$\rho_p = \frac{\pi \times L_\lambda \times d^2}{\text{ESUN}_\lambda \times \cos \theta_s} \quad (6)$$

where ρ_p is unitless planetary reflectance, L_λ is spectral radiance at the sensor's aperture, d is the Earth–Sun distance in astronomical units, ESUN_λ is the mean solar exoatmospheric irradiances, and θ_s is the solar zenith angle.

Decision tree classifier

A simple thresholding decision tree (DT) classifier was created to combine and transform the satellite data into rice map products (Figure 2). DTs have substantial advantages for remote sensing classification problems because of their flexibility, intuitive simplicity, and computational efficiency (Friedl and Brodley, 1997; Defries et al., 1998; Brown et al., 2003). DTs predict class membership by recursively partitioning data into more homogenous subsets. To automate the processing, an operational approach was carried out for possible long-term or large-area monitoring. A series of nodes were created that seamlessly combined the satellite data to extract the strengths of the SAR and optical sensors. Figure 2 highlights the primary inputs, work flow, and nodes that generate rice information. Each node in the DT informs the next node for more thorough rice information.

Training areas at locations where field data were collected were used to generate threshold limits that were then



automated in the DT. To automate this process, all pixels had image statistics extracted from the multitemporal ScanSAR WB1 data (10 ScanSAR images total; once every 46 days for the 2007 calendar year with adjacent paths having a 50% overlap). For each pixel, the minimum, maximum, and dynamic range of SAR backscatter values (σ^0) were extracted (first with training areas, then applied to other regions) to represent water (inundated fields and natural water bodies) and rice phenology (biomass growth) within the DT. The DEM was used at this node as a mask to eliminate any pixel over a 3% slope from being classified as rice. Three percent was chosen to allow for potential error in the DEM and masked obvious errors in a qualitative assessment. The majority of paddies in this region surround the lake areas so little to no isolated upland terraced paddies were disregarded with the resolution of the DEM and slope threshold. Also at this node the Landsat water mask was applied to eliminate potential confusion between rice paddies and natural water or wetland areas. The Landsat mask was developed from an overpass date that corresponded to the high water period of Poyang Lake during the dormant rice crop season. At this node in the DT a rice extent map was created (Figure 2).

For each pixel classified as rice, a suite of agro-ecological attributes were extracted based on multitemporal MODIS and PALSAR observations to identify rice paddy characteristics (i.e., cropping intensity). Time-series analysis characterizing changes in phenology and flooding over time was carried out with both PALSAR and MODIS to assess cropping intensity, hydroperiod, and crop calendar. Rice phenology can be divided into primary stages: flooding, transplanting, seedling development, tillin, heading, maturation, and harvesting. The regional growing season of rice crops is approximately 90–120 days depending on the number of crops (single, double, triple) and the genetic strain planted. For example, in a typical double-crop system

in the region, flooding occurs at least 1 week before planting. Planting occurs around DOY 100 for the first crop and 190 for the second crop. Using the knowledge of the hydroperiod and rice growth, a crop calendar was generated by deriving the frequency of flooding and the growth cycle for the paddy. From the number of hydroperiod events the number and timing of crops can be determined. The dates of activity (flooding, harvest) were then mapped for the rice paddies to monitor crop calendar and crop intensity (i.e., single, double, triple).

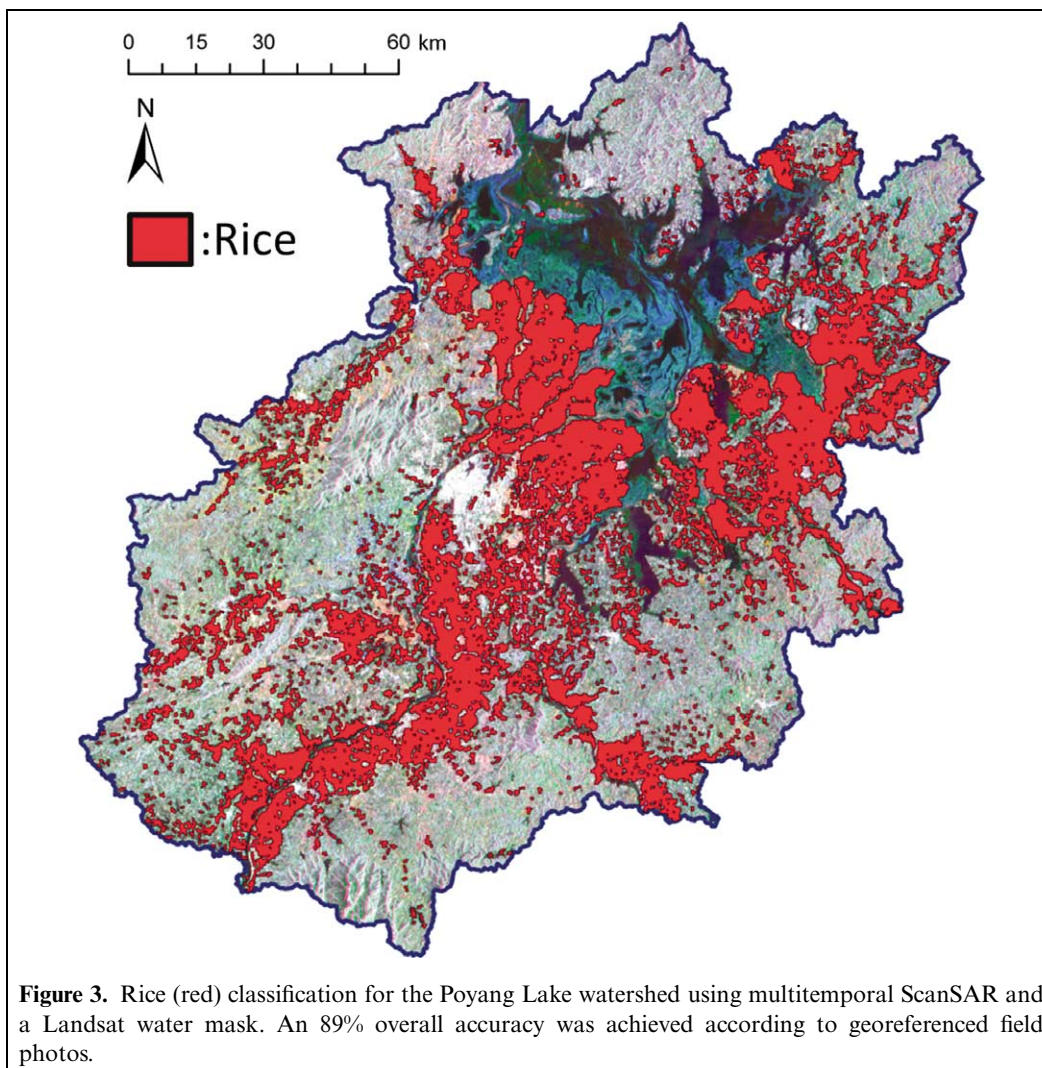
Results and discussion

The DT approach effectively mapped rice agro-ecological paddy attributes. The first primary two nodes in the DT keyed off water and rice biomass growth using the pre-processed ScanSAR. Average values from the five training paddies using the multitemporal ScanSAR were obtained for the DT node to map rice extent. The values (σ^0) used in the DT for minimum and maximum were -11 and -6.0 , respectively, with dynamic range equal to the difference. To

remove potential misclassifications the Landsat lake- and SRTM-masks were applied at the next node to eliminate topographic and wetlands confusion. At this stage in the DT the rice paddy extent map was created.

In the defined PLW, 5862 km² were classified as rice paddies (Figure 3). This equates to classifying approximately 25% of the watershed as rice agriculture. The most intense regions of rice were adjacent to the southwestern coastline of the lake among tributaries of the Fuhe River and the delta-like features of the Ganjiang River extending toward the city of Nanchang. Near-continuous rice paddies occupy the landscape immediately adjacent to the southeastern coastline among tributaries of the Xinjiang and Pojiang rivers as well.

Jiang et al. (2008) classified approximately 45% of their PLW region as farmland in 2004 using Landsat imagery. Rao et al. (2002) classified approximately 40% land area as farmland. Jiang et al. (2008) and Rao et al. (2002) combined rice with upland crops, such as orchards and vegetables, to reduce confusion; therefore, the different classification schemes have a noteworthy difference when comparing the



findings from this study to other recent Poyang Lake region classifications. Considering differences in the classification schemes, objectives, data, and temporal and spatial scales, the proportional totals of the classified rice areas generated in this study are generally consistent with other recent classifications.

From the ground truth field campaign a simple 2×2 binary matrix (rice vs. not rice) was generated to provide an overall accuracy for the rice map. We chose to carry out a simple contingency table as no other land covers were identified from the DT that mapped rice paddy attributes. A total of 320 georeferenced field photos were categorized, and an overall accuracy of 89% (286/320) was achieved. This represents a high overall accuracy considering the scale of the data and the heterogeneous region classified. The high accuracy might be attributed to the fact that ground control points were stratified among aquatic habitats; however, these are most likely the types of land use and covers that would be most confused with rice paddies. It is possible that small and isolated rice paddies in higher elevations and more complex topographies (of which there is very little in PLW) were under- or misclassified. However, no anecdotal evidence showed this to be the case.

We believe the relatively high accuracy (>85%; Foody, 2002) was achieved in part due to the PALSAR acquisition strategy and DT classifier. First, the multitemporal observations enabled the capture of key phenological patterns that are unique to rice. Few, if any, land types have patterns of growth and land management (i.e., flooding) that are similar to rice crops and their respective backscatter signal. The bounce patterns of rice and erectly oriented aquatic vegetation with L-band SAR has been well established (i.e., Inoue et al., 2002). Second, the Landsat water mask created during a high water event prevented numerous potential misclassifications because of dynamic lake wetland regions. While a small amount of rice paddies immediately adjacent to lake wetlands and riparian areas might have been underclassified this resulted in higher accuracy by eliminating misclassified coastal wetlands as desired. However, the georeferenced field photos provided no evidence that these regions were actually underclassified. These results show that the operational approach can be executed with little to no a priori data to generate rice maps with multitemporal observations ScanSAR data.

The field data were collected to calibrate the paddy attribute algorithms during the 2007 rice season. **Figure 4** illustrates the relationship between the paddy parameters and remote sensing metrics during a “typical” double crop. Irrigation from canals precedes transplanting, and the inundation status between crops within the same calendar year was shorter according to both the field measurements and the remotely sensed hydroperiod metric. **Figure 4** shows the inundation period between early and late rice in the double crop system was half as long (approximately 2 consecutive 8-day periods). In fact the hydroperiod for the initial flooding for early rice was 8 consecutive 8-day periods

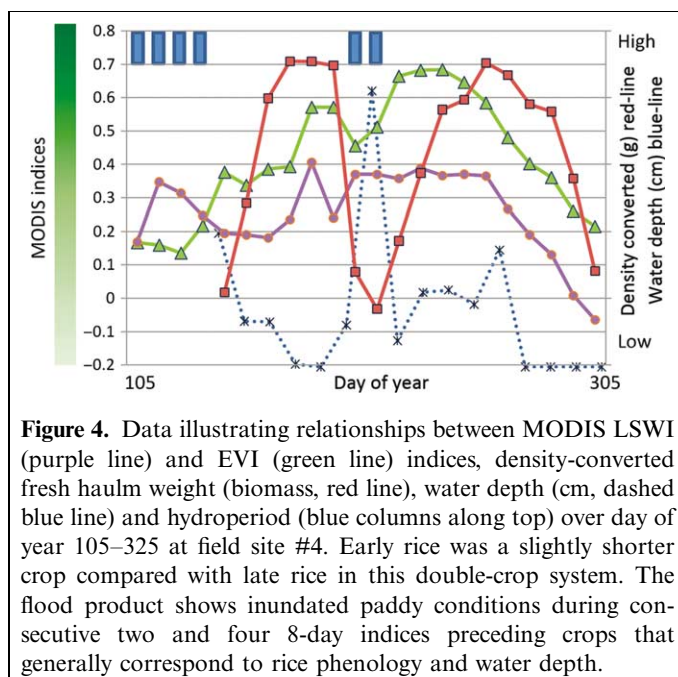


Figure 4. Data illustrating relationships between MODIS LSWI (purple line) and EVI (green line) indices, density-converted fresh haulm weight (biomass, red line), water depth (cm, dashed blue line) and hydroperiod (blue columns along top) over day of year 105–325 at field site #4. Early rice was a slightly shorter crop compared with late rice in this double-crop system. The flood product shows inundated paddy conditions during consecutive two and four 8-day indices preceding crops that generally correspond to rice phenology and water depth.

at our corresponding field site; however, the data shown in **Figure 4** begins closer to early crop transplanting as this is when field data collection began. MODIS flood pixels at site four began on DOY 73 and the paddy remained inundated until DOY 129 for a 56-day hydroperiod. As biomass increases, the EVI signal increases, which causes the LSWI signal to decrease. Once a biomass and EVI threshold are reached, the MODIS flood product has difficulty detecting water beneath maturing rice.

Biomass and water depth tended to be inversely related, as expected. As the growing season progresses and the rice matures, the water depth decreases toward harvest when paddies are fully drained. Some spikes in water depth are noted. Changes in water depth can be caused by a number of factors, including water management, soils, and evapotranspiration (ET) losses. Typically, farmers will flood fields to a depth of >10 cm when they transplant rice. Over time the depth of the water decreases because of leaching and ET losses. Depending on the rate of loss, farmers may or may not reflood before intentionally draining the field prior to harvest. The water depth and MODIS flood signal between early and late rice correspond well. As the paddy was flooded for the second crop in the double rice system, LSWI approached EVI to indicate flood conditions. In the longer flood period before early rice LSWI consistently remained higher than EVI.

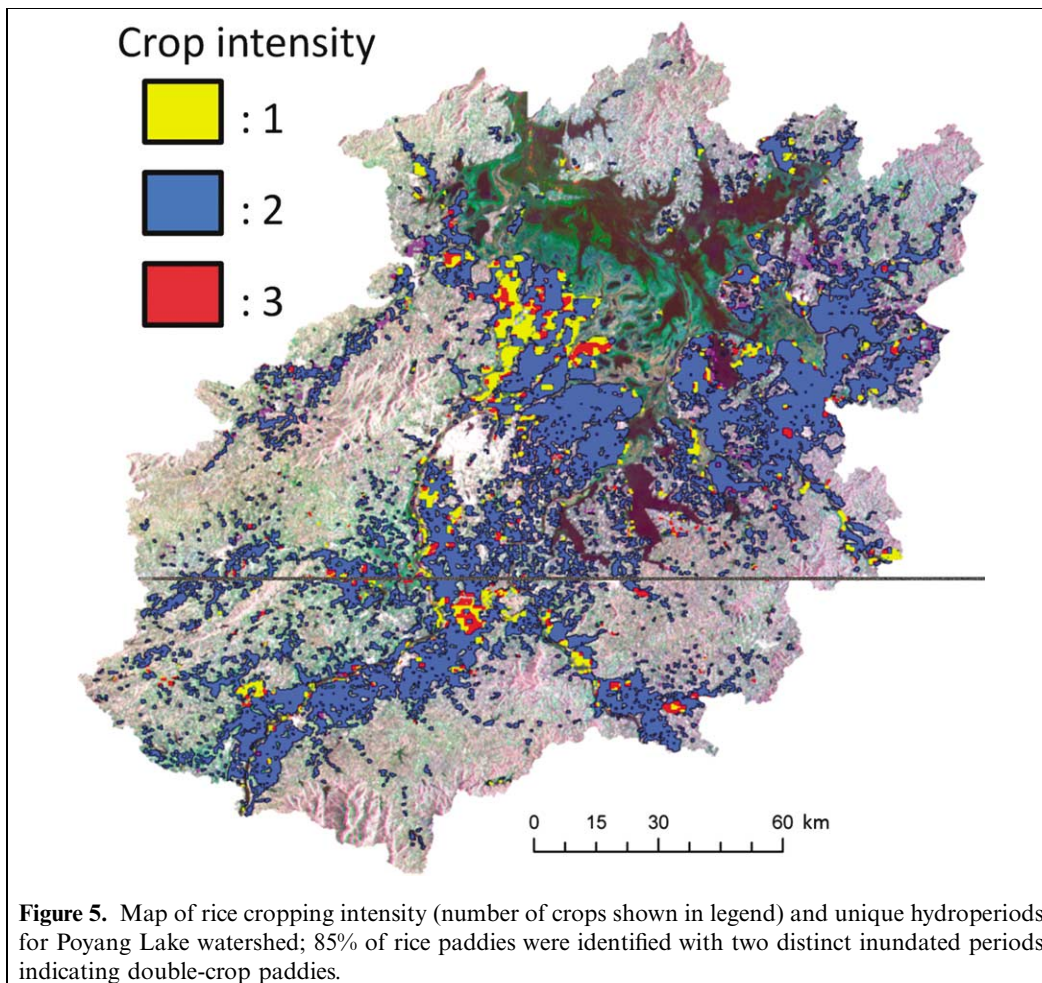
Though the amplitudes are slightly different, EVI and biomass appear generally related and follow similar trends. Some lag is apparent between EVI and the second rice crop at the illustrated field site (**Figure 4**). Some variability and noise are likely introduced when scaling from plot level data to MODIS pixels at a resolution of 500 m and because the composites are from a range of possible days over an 8-day period. The man-made bunds (primary “walls” separating

main rice fields and irrigation channels) and the paddy checks (smaller secondary man-made “walls” within fields creating smaller paddies) that delineate fields into smaller individual rice paddies contribute to mixed pixel issues at the 500 m scale. Most likely isolated and patchy landscapes or terraced rice areas would be more challenging to monitor compared with large, near-continuous scale paddies. The rice areas in the PLW primarily have a large area (adjacent to lake and major tributaries), are flat, and are similarly managed, which reduces mixed signal problems.

After the rice extent node, the high frequency MODIS was used to generate hydroperiod status at 8-day intervals for 2007. Approximately 85% of the rice paddies had two distinct hydroperiods, defined as at least two consecutive MODIS flood ($LSWI + 0.05 > EVI$) observations during the rice growing season (approx. DOY 81–329) in the watershed (Figure 5). The 85% indicates that the majority of paddies were in a double-crop intensity scheme. In other words, inundation periods are a signal of the crop cycles, and two distinct and mutually exclusive inundation periods indicate a two-crop pattern; an early crop and a late crop dominate rice management in the PLW. Four percent and three percent were found to be triple and single crop, respectively. The operational approach allowed for the continuous

mapping of the hydroperiod. This permits a better understanding of irrigation patterns and water resources.

Dates for crop calendar monitoring using MODIS and ScanSAR covered observations between DOY 80 and 330. Five ScanSAR observations were DOY 103, 149, 190, 241, and 287. The MODIS observations covered 248 days with 31 8-day measurements with a start date of 22 March 2007 and an end date of 25 November 2007. Using the rice extent node in the DT, the thresholds were used to characterize phenological changes in rice paddies (measurements of rice growth, harvest, and flooding during the rice season). The temporal thresholds that were set created filters that did not allow erroneous crop and flood patterns. For example, rice crops take a period of time to grow (i.e., 90 days) and therefore multiple crops or flood signals cannot exist within a period less than a crop cycle (i.e., no 45 day crops). By temporally aggregating the number of crops and flood cycles the crop calendar was derived. The hydroperiod mapping approach that relies on high (temporal) frequency has been shown to be accurate in multiple rice ecosystems including Vietnam, China, and California, USA (Xiao et al., 2005; Sakamoto et al., 2008; Torbick et al., 2010). Therefore, this operational approach can be executed for any region with no a priori data. As indicated in Figure 4 the crop



calendar attributes generally coincided with the field-level measurements. Obtaining crop calendar field data for large regions is a challenge, and future efforts will continue to gather ground truth calendar data.

Conclusion

The operational approach to monitoring rice agriculture has the potential to contribute to a GEOSS framework integrating SAR and optical sensors. The integrated PALSAR and MODIS found that the PLW was 25% rice agriculture. Georeferenced ground truth field photos found the operational rice extent product to have 89% overall accuracy. The MODIS hydroperiod index found that 85% of rice in the watershed underwent a double-cropping intensity pattern with inundation periods for early rice that were twice as long as the inundation period for late rice. The DT model indicated that planting and harvest dates were found to occur approximately around DOYs 77 and 329. The acquisition strategies of these sensors will enable more thorough agro-ecological attributes to be assessed at the regional scale. The ability to characterize hydroperiods, cropping intensity, and calendar information can potentially provide decision makers with timely information to assess the impacts of disasters, policies, and management patterns. This approach needs to be further validated in other environments to more thoroughly evaluate capabilities in ranging environmental conditions such as complex topography. Continued acquisitions and data continuity are critical for establishing longer-term monitoring frameworks, and data access will remain crucial.

Acknowledgements

We would like to thank the GEO community for holding the SAR agriculture workshop in Kananaskis, Alberta, Canada, 2–4 November 2009. This work was undertaken within the framework of the JAXA Kyoto & Carbon Initiative. ALOS PALSAR data were provided by JAXA EORC. Additional support was provided by the NASA LCLUC (#NNX08AL16G) and the National Institute of Health (NIH) Fogarty International Center (R01-TW007869), and the China Ministry of Science and Technology (CMOST) Special Program for Prevention and Control of Infectious Diseases (No. 2008ZX10004-012).

References

Brown de Colstom, E., Story, M., Thompson, C., Commisso, K., Smith, T., and Irons, J. 2003. National park vegetation mapping using multitemporal Landsat 7 data and a decision tree classifier. *Remote Sensing of Environment*, Vol. 85, No. 3, pp. 316–327. doi: 10.1016/S0034-4257(03)00010-5.

Congalton, R., and Green, K. 1999. *Assessing the accuracy of remotely sensed data: Principles and practices*. Lewis Publishers, New York.

Defries, R., Hansen, M., Townsend, J., and Sohlberg, R. 1998. Global land cover classification at 8 km spatial resolution: the use of training data derived from Landsat imagery in decision tree classifiers. *International Journal of Remote Sensing*, Vol. 19, No. 16, pp. 3141–3168. doi: 10.1080/014311698214235.

Erasmi, S., and Twele, A. 2009. Regional land cover mapping in the humid tropics using combined optical and SAR satellite data: a case study from Central Sulawesi, Indonesia. *International Journal of Remote Sensing*, Vol. 30, No. 10, pp. 2465–2478. doi: 10.1080/01431160802552728.

ERSDAC. 2006. *PALSAR User's Guide*. Earth remote sensing data analysis center (ERSDAC). Available at http://www.palsar.ersdac.or.jp/e/guide/pdf/U_Guide_en.pdf [accessed October 2009].

Foody, G.M. 2002. Status of land cover classification accuracy assessment. *Remote Sensing Environment*, Vol. 80, pp. 185–201.

Friedl, M., and Brodley, C. 1997. Decision tree classification of land cover from remotely sensed data. *Remote Sensing of Environment*, Vol. 61, No. 3, pp. 399–409. doi: 10.1016/S0034-4257(97)00049-7.

Gilbert, M., Xiao, X., Domenech, J., Lubroth, J., Martin, V., and Slingenbergh, J. 2008. *HPAI spread from the western Siberian lowland to the eastern Mediterranean and beyond*. Consultancy report for the Animal Health Division, Food and Agriculture Organization of the United Nations, Rome, Italy.

Huete, A., Didan, K., Miura, T., and Rodriguez, E. 2002. Overview of the radiometric and biophysical performance of the MODIS vegetation indices. *Remote Sensing of Environment*, Vol. 83, No. 1–2, pp. 195–213. doi: 10.1016/S0034-4257(02)00096-2.

Inoue, Y., Kurosu, T., Aeno, H., Uratsuka, S., Kozu, T., Dabrowska-Zielinska, K., and Qi, J. 2002. Season-long daily measurements of multifrequency (Ka, Ku, X, C, and L) and full-polarization backscatter signatures over paddy rice field and their relationship with biological variables. *Remote Sensing of Environment*, Vol. 81, No. 1–3, pp. 194–204. doi: 10.1016/S0034-4257(01)00343-1.

Intergovernmental Panel on Climate Change (IPCC). 1992. *Climate Change: The Supplementary Report to the IPCC Scientific Assessment*. Cambridge University Press, New York.

Jarvis, A., Reuter, H.I., Nelson, A., and Guevara, E. 2008. Hole-filled seamless SRTM data V4, International Centre for Tropical Agriculture (CIAT), Available from <http://srtm.csi.cgiar.org> [accessed October 2009].

Jiang, L., Berge, K., Brown, D., Zhao, T., Tian, Q., and Qi, S. 2008. Land-cover change and vulnerability to flooding near Poyang Lake, Jiangxi Province, China. *Photogrammetric Engineering & Remote Sensing*, Vol. 74, pp. 1–12.

Justice, C., and Becker-Reshef, I. 2007. Developing a strategy for global agricultural monitoring in the framework of the Group on Earth Observations Workshop Report, 16–18 July 2007, FAO, Rome.

Li, C., Frohling, S., Xiao, X., Moore, B., Boles, S., Qiu, J., Huang, Y., Salas, W., and Sass, R. 2005. Modeling impacts of farming management alternatives on CO₂, CH₄, and N₂O emissions: A case study for water management of rice agriculture in China. *Global Biogeochemical Cycles*, Vol. 19, No. xxx, pp. xxx. doi:10.1029/2004GB002341.

Liang, S. 2005. *Topographic correction methods: Quantitative remote sensing of land surfaces*. John Wiley & Sons, Inc. 10.1002/047172372X.

Liu, X., Chen, M., Chen, W., Huang, L., and Xiao, Z.H. 2005. Variation of cultivated land and its driving forces in Poyang lake area. *Journal of Jiangxi Agricultural University*, Vol. 27, pp. 309–312.

- McNairn, H., Champagne, C., Shang, J., Holmstrom, D.A., and Reichert, G. 2009. Integration of optical and Synthetic Aperture Radar (SAR) imagery for delivering operational annual crop inventories. *Journal of Photogrammetry and Remote Sensing*, Vol. 64, No. 5, pp. 434–449. doi: 10.1016/j.isprsjprs.2008.07.006
- National Bureau of Statistics (NBS). 2000. *China Statistical Yearbook*. Beijing: National Bureau of Statistics.
- Parihar, J. 2009. *The GEO Agricultural Monitoring Community of Practice*. International GEO workshop on Synthetic Aperture Radar to support agricultural monitoring. 2–4 November, 2009, Kananaskis, Alta., Canada.
- Pradhan, S. 2001. Crop area estimation using GIS, remote sensing and area frame sampling. *International Journal of Applied Earth Observation and Geoinformation*, Vol. 3, No. 1, pp. 86–92. doi: 10.1016/S0303-2434(01)85025-X.
- Rao, S., Fang, J.Y., Cui, H.T., and Lei, G.C. 2002. Spatio-temporal changes in patterns of land-use in Poyang Lake during the last decade. *Resources and Environment in the Yangtze Basin*, Vol. 11, No. 5, pp. 421–426.
- Rosenqvist, A., Shimada, S., and Watanbe, M. 2004. ALOS PALSAR: Technical outline and mission concepts. 4th International Symposium on Retrieval of Bio- and Geophysical Parameters from SAR Data for Land Applications, Innsbruck, Austria, 16–19 November 2004.
- Sakamoto, T., Yokozawa, M., Toritani, H., Shibayama, M., Ishitsuka, N., and Ohno, H. 2008. Spatio-temporal distribution of rice phenology and cropping systems in the Mekong Delta with special reference to the seasonal water flow of the Mekong and Bassac rivers. *Remote Sensing of Environment*, Vol. 100, No. 1, pp. 1–16. doi: 10.1016/j.rse.2005.09.007.
- Salas, W., Boles, S., Li, C., Yeluripati J., Xiao, X., Frohling, S., and Green, P. 2007. Mapping and modeling of greenhouse gas emissions from rice paddies with satellite radar observations and the DNDC biogeochemical model. *Aquatic Conservation: Marine and Freshwater Ecosystems*, Vol. 17, No. 3, pp. 319–329. doi: 10.1002/aqc.837.
- Torbick, N., Xiao, X., and Salas, W. 2010. Monitoring rice agriculture in the Sacramento Valley, USA using multitemporal PALSAR and MODIS imagery. *Journal of Selected Topics in Remote Sensing*, doi: 10.1109/JSTARS.2010.2091493.
- Xiao, X.M., Boles, S., Liu, J.Y., Zhuang, D.F., Frohling, S., Li, C., et al. 2005. Mapping paddy rice agriculture in southern China using multi-temporal MODIS images. *Remote Sensing of Environment*, Vol. 95, No. 4, pp. 480–492. doi: 10.1016/j.rse.2004.12.009.
- Xiao, X., Boles, S., Frohling, S., Li, C., Badu, J., Salas, W., and Moore, B. 2006. Mapping paddy rice agriculture in South and Southeast Asia using multi-temporal MODIS images. *Remote Sensing of Environment*, Vol. 100, pp. 95–113. doi: 10.1016/j.rse.2005.10.004.